D35

M trology of subwav l ngth photor sist gratings using optical scatt rometry

Christopher J. Raymond, Michael R. Murnane, S. Sohail H. Naqvi, and John R. McNeil
The Center for High Technology Materials, The University of New Mexico, Albuquerque,
New Mexico 87131

The widths and overall profiles of dielectric grating lines can be determined by measuring the intensity of diffracted laser light from the sample over a specified range of incident beam angles. This technique, known as 2-Θ scatterometry, is able to accurately and precisely measure photoresist structures in the subhalf micron regime. Moreover, a 2-Θ scatterometer is capable of making measurements in a rapid and nondestructive manner. To test this technique we measured five identically processed wafers with nominal 0.5 μm line/0.5 μm space grating patterns. Each wafer comprised gratings in a Shipley 89131 negative photoresist exposed in a matrix of incremental exposure doses and focus settings. The scatterometry results were consistent with cross-sectional and top-down scanning electron microscopy (SEM) measurements of the same structures. The average deviation of 11 scatterometer linewidth measurements from top-down SEM measurements, over a broad exposure range, is 14.5 nm. In addition, the repeatability (1σ) of the 2-Θ scatterometer is shown to be excellent: 0.5 nm for consecutive measurements and 0.8 nm for day-to-day measurements. © *1995 American Vacuum Society.*

I. MICROELECTRONICS METROLOGY: AN OVERVIEW

As the integration and speed of microelectronic devices increase, the dimensions of circuit structures must continue to decrease in size and to improve in terms of profile edge acuity. High-end devices such as microprocessors require a considerable number of process steps. Therefore, it is becoming increasingly important to have an accurate, quantitative description of the submicron structure present at each step. This places increasing demands on present-day metrology techniques, and, at present, there is no single technique capable of meeting all of these demands. Furthermore, there is a growing need for wafer process monitoring and closed loop control, both of which would require in-line sensors. In addition, these wafer/process sensors must be integrated into the fabrication line, i.e., they must have a reasonable footprint and be able to monitor the process rapidly. Most linewidth measurement equipment is either too slow or too complex to be implemented in an in-line arrangement for high-throughput wafer evaluation. An ideal in-line metrology technique or sensor would be capable of making measurements that are sufficiently accurate, repeatable, and rapid at a low cost.

The major tools at the disposal of the semiconductor industry include electrical measurements, optical microscopy, various probe microscopy techniques, and scanning electron microscopy (SEM). Each technique has its strengths and weaknesses, and many in industry believe that these metrologies will be used in a complementary fashion to exploit the potential of each.

Electrical testing is a useful method for testing submicron features under certain conditions. The most appealing attributes of electrical methods include 6 nm precision (3σ)[1] and the ability to measure critical dimensions as small as 0.2 μm. A major limitation is the fact that measurements must be

made on a conducting film after the etching step when reworking the wafer is less feasible.[1,2] In addition, because it involves contact, it is slow and not amenable to in-line applications.

Optical microscopy still plays an important role in submicron metrology due to its versatility, simplicity, and speed.[1] Sectioning optical microscopes have received much attention lately for achieving three-dimensional imaging of submicron structures, an attractive feature for overlay measurement.[1] The two predominant types of sectioning optical microscopes are confocal scanning optical microscopes (CSOMs) and interference effect microscopes.[3] One of the most attractive features of optical microscopes is that they do not require placing the sample in a vacuum, a fact that translates into lower cost relative to most competing metrologies. Unfortunately, traditional microscope designs suffer in terms of resolution and precision when measuring structures at or below 0.5 μm.[4] Improvements in technique, design, and materials, however, may continue to improve accuracy and repeatability and thus keep optical microscopy a viable metrology. Diffraction limitations are driving optical microscope design into scanning near-field optical microscopy (SNOM)[4,5] which allows for high-resolution imaging. It is important to note that SNOMs can also be classified as probe microscopes,[6] another metrology for making three-dimensional measurements.

Although in general probe-type instruments are capable of high resolution in three dimensions, the measurement process is slow. Furthermore, the image obtained is difficult to interpret unless the tip shape is well known.[6] Probe tips must be highly specialized for the type of topography to be scanned and, in some cases, especially when high aspect ratio features are involved, portions of the profile can be inaccessible to the probe. Scanning tunneling microscopes (STMs) are a special class of probe microscopes capable of atomic resolution in a high vacuum. There are two major

drawbacks to direct-current tunneling microscopes; they cannot measure nonconductive samples and close contact between the probe and the sample results in forces that can alter both.[6]

Samples measured with atomic force microscopes (AFMs) need not be coated with a metal because no current flows from the probe to the sample. Atomic resolution has been reported for AFMs operating in repulsive mode,[6–10] where the probe–sample distance is on the order of 1 nm or less. As the probe–sample separation increases, probe–sample forces become attractive and resolution generally decreases. Recent literature reports lateral resolutions in the 5–10 nm range.[11] One drawback to using an AFM is that the probe tip must be frequently and accurately characterized, a tedious process that is not always practical.

SEMs, which offer greater resolution than optical microscopes, are becoming the standard metrology technique for the semiconductor industry.[12] The enhanced resolution comes at a price, however; samples must be measured in a high vacuum, thereby increasing the complexity and cost of each measurement and limiting throughput.[1] In the case of samples with insulating structures, charging effects and electron absorption can cause measurement errors and sample damage, respectively.

Top-down, or line-scan (LS) SEM measurements can provide linewidth information with the use of an appropriate edge detection algorithm. Although the use of different edge detection algorithms has lead to inconsistent results,[13] recent improvements in electron–sample interaction models are enabling researchers to make more accurate characterizations. By incorporating backscattered electron (BSE) models and Monte Carlo algorithms, edge positions have been located to within 10 nm, and sensitivity to rough and rounded profiles has been demonstrated.[14] Backscattered electron imaging has also been reported capable of measuring high aspect ratio resist features with a 3σ precision of 4 nm.[15] The calibration of SEMs for linewidth measurement, however, has been difficult due to the lack of availability of a standard.[16] Furthermore, top-down linewidth measurements on nonsquare profiles that do not have a well-defined vertical edge, can be misleading.[11]

Scanning electron microscopes can also be operated in "cross-section" (CS) mode. While this approach allows for complete line shape characterization, studies have indicated that the systematic error of a CS scan is larger than that of a top-down SEM measurement under the same operating conditions. This is thought to be a consequence of different contrast formation mechanisms that result from the different sample geometries of the LS and CS modes. The distortions introduced in CS mode can cause errors that transcend the linewidth tolerances permitted for subhalf micron structures.[17] Furthermore, cross sectioning obviously destroys the wafer, a drawback that rules this technique out for high volume, in-line applications.

Diffraction-based analysis techniques[18] such as scatterometry are especially well suited for microelectronics metrology applications because they are nondestructive and rapid.[19] These metrology techniques have already proven useful in a variety of microlithographic applications, including

alignment,[20] overlay,[21] temperature measurement,[22] monitoring of latent image focus,[23] exposure,[24] and postexposure bake.[25] Scatterometry has shown promise as an accurate, repeatable, and inexpensive alternative to other metrologies.[19] With its sensitivity, versatility, and capability of high-throughput measurement, scatterometry is gaining recognition as a potentially powerful metrology of the very near future.

II. SCATTEROMETRY

Scatterometry is the angle-resolved measurement and characterization of light scattered from a structure. For structures that are periodic, incident light is scattered or diffracted into different orders. The angular location θ_f of the mth diffraction order with respect to the angle of incidence θ_i is specified by the grating equation

$$\sin \theta_i + \sin \theta_f = m\frac{\lambda}{d}, \tag{1}$$

where λ is the wavelength of incident light and d the period of the diffracting structure.

The diffracted light pattern from some structure can be used as a "fingerprint" or "signature" for identifying the dimensions of the structure itself. In addition to period, which can be determined quite easily, more specific dimensions such as the thickness of the photoresist, angle of the sidewalls, and width of the line can also be measured by analyzing the scatter pattern.

The scatterometric analysis can best be defined in two steps. First, the diffracted light fingerprint is measured. This is known as the forward problem. The second step, the inverse problem, consists of determining the shape of the grating that scatters the incident light. To solve this problem, the grating shape is parameterized[26] and a parameter space is defined by allowing each grating shape parameter to vary over a certain range. A rigorous diffraction model[27] is used to calculate the diffracted light fingerprint from each grating in the parameter space, and a statistical prediction algorithm is trained on this theoretical calibration data. Subsequently this prediction algorithm is used to determine the parameters that correspond to the fingerprint found in the forward problem.

In our work discussed here, the forward problem is solved using a 2-Θ scatterometer, seen in Fig. 1. A simple He–Ne laser beam, $\lambda = 633$ nm, is incident upon a sample after it passes through a spatial filter and some focusing optics. The sample is mounted on a stage that permits it to rotate. Since the beam itself is fixed, this rotation changes the angle of incidence on the sample. Using grating Eq. (1), the detector arm of the scatterometer is able to follow any diffracted order as this angle is varied. The intensity of a particular diffraction order as a function of incident angle, which is known as a 2-Θ plot or scatter "signature," is then downloaded to a computer, where the analysis can begin.

Previous scatterometry applications on large period samples measured the entire diffraction order envelope at a fixed angle and used this as a means for determining the dimensions of the scattering structure.[26,28] But, for 1 μm period gratings, the size of interest for this study, only the 0th
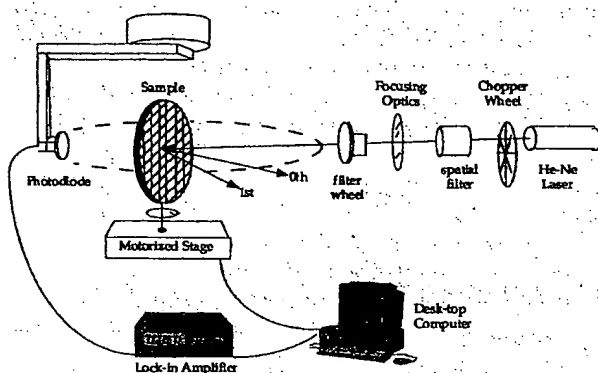
FIG. 1. The 2-Θ scatterometer experimental arrangement.

approximate an infinite structure.[30] Thus, for a 1 μm pitch grating, the beam must have a diameter of at least 20 μm.

It is important to note a major difference between measurements made by scatterometry and those made by other methods. Because the spot size of the incident beam is much larger than the period of the diffracting structure, many lines and spaces are illuminated and all contribute collectively to the diffraction signal. Therefore, line shape characterization values using scatterometry are averages of all the illuminated structures. This averaging effect can be an advantage because a SEM photo may depict a structure that is not representative of the entire sample. The spot size of the scatterometer can be adjusted to measure the average line shapes of hundreds of features or a localized group of them. This illustrates how competing technologies are often complementary in certain respects.

and ±1st diffraction orders exist over a practical angular range. Measuring this diffraction envelope, then, does not provide the data required for an accurate analysis. However, a 2-Θ plot contains enough information for proper characterization of the diffracting structure and may be thought of as a fingerprint of that structure. For example, Fig. 2 shows two 2-Θ plots of the zeroth order intensity in which the linewidth of a 1 μm pitch grating is changed by 10 nm.

The scatterometer's laser was TE polarized for this study. To enhance the signal-to-noise ratio and minimize error, a conventional lock-in detection system is used. The beam spot size on our sample was approximately 400 μm for ease of use, but can be made smaller, and if changed, does not affect the diffraction efficiency.[24,29] One important consideration regarding spot size is the number of grating periods illuminated by the beam. Theory assumes the structure is infinitely wide, in practice, 20 or so illuminated period are sufficient to

III. DIFFRACTION MODEL

With the acquisition of experimental diffraction data using the 2-Θ scatterometer, the forward problem is complete. The next step in the overall analysis strategy is to generate a series of theoretical diffraction data so that the inverse problem may be solved. This requires a diffraction model.[27]

For structures which are periodic in one dimension, these theoretical diffraction "signatures" can be constructed using the rigorous coupled wave theory (RCWT) developed by Gaylord and Moharram.[31] This vector differential technique uses Maxwell's equations and the appropriate boundary conditions at all interfaces to solve for the electric fields in each region of the sample. The total reflected field intensity can then be calculated; it is comprised of discrete diffracted "orders" as a result of the periodic structure, as is evidenced by grating Eq. (1) presented earlier. The RCWT diffraction
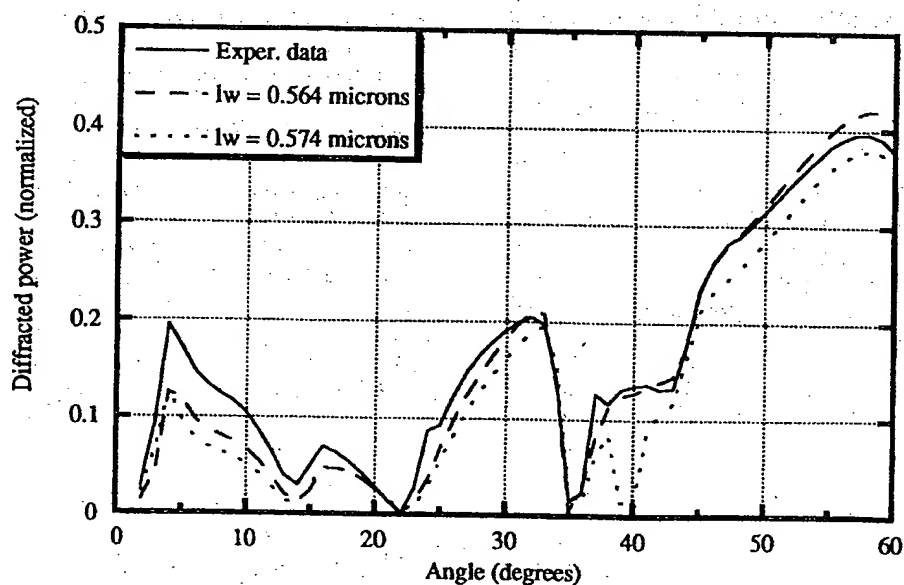

FIG. 2. Theoretical 2-Θ scans of the zeroth order for two different linewidths that differ by 10 nm and the experimental data that best agrees with the smaller linewidth.

model is particularly useful for photoresist grating applications because it can account for nonsquare grating profiles, discussed later in Sec. VI, as well as any number of underlying film layers or substrates. A complete overview of rigorous coupled wave theory with respect to scatterometric applications can be found in Naqvi et al.[27]

The generation of theoretical scatter signatures is the most time-consuming process of the entire scatterometric analysis. For example, it takes approximately 30 s for a Hewlett-Packard (HP) Apollo workstation to generate one 2-Θ signature for a square grating profile. Most of the analyses presented here required some 400 signatures, resulting in 3.33 h of computation time. It is important to note that, for a given parameter space, the calibration procedure only needs to be performed once.

IV. STATISTICAL ANALYSES/PREDICTION ALGORITHMS

Once the theoretical database has been generated, the second part of the inverse problem, namely, characterizing the diffracting structure, begins. The partial least squares (PLS) algorithm of Chemometrics, a multivariate analysis package, was selected as one means for solving the inverse problem based on its success in the past[26,32] and its good performance over a wide range of experimental conditions.[33] A detailed description of Chemometrics is given by Haaland et al.[34]

With PLS, the statistical solution of the inverse problem occurs in two phases. In the calibration phase, either empirical or theoretically generated diffraction order intensity data are used to train a prediction model. All of the results presented in this article involve the prediction of line shapes, and thus it was possible to generate the theoretical data sets using RCWT. If we had wished to predict stepper settings such as exposure dose or focus setting, measurements on gratings exposed at each value in the focus–exposure matrix would have been taken. These data would then be used as the calibration set to predict focus and exposure dose on unknown samples. In the second phase, the parameters of interest of the unknown sample are predicted using the model derived from the calibration set. The prediction step is very rapid, allowing for a nearly instantaneous characterization of the unknown sample.

Another technique for solving the inverse problem is through the use of minimum mean square error (MMS) analysis. Like Chemometrics, the foundation for MMS analysis is in the calibration set, which, again, can utilize either empirical or theoretical data for training. The actual analysis proceeds by comparing an unknown experimental intensity data file with each file in the calibration set. The mean square error is calculated for each comparison, and the closest match (minimum mean square error) recorded. The linewidth or overall line shape associated with the closest calibration file is taken to be the parameters of the unknown structure.

Both PLS and MMS have performed well in our analyses. The method of choice depends on the application involved. Typically MMS works better when intensity data are only weakly affected by a change in a given parameter. One ex-

ample is the slight change in diffracted power caused by slightly rounded corners on photoresist lines. In addition, the actual minimum mean square error returned by the algorithm is a direct indicator of how well theory and experiment agree and this error value serves as a confidence level of the prediction. However, MMS is not capable of interpolating between calibration data points as is PLS. Still, MMS has proven to be more dependable if the computing power is available to create a calibration set of sufficient resolution. Another potential pitfall in using MMS is that it is not sufficiently sophisticated to recognize data outliers; it simply determines the difference between theory and experiment at each data point and does not account for similarities and/or differences between two sets of data.

Chemometrics/PLS actually builds a calibration model based upon an input calibration data set. Using this calibration model, it is able to notice trends in data and predict an unknown parameter, even to the point of interpolating between calibration data based on those trends. Chemometrics also has built-in statistical returns that serve as confidence indicators for the prediction. However, when parameter changes manifest themselves only slightly in the scatter signature, Chemometrics has not performed well.

We have also evaluated the impact of the range of incident angles on the effectiveness of the prediction. In principle the 2-Θ scatterometer can take data on any diffraction order for incident angles ranging from −90 to +90°. In practice, however, we have limited the angular range to ±60°; at angles much beyond this the incident light is almost completely reflected and contains little information about the structure (i.e., the zeroth order intensity approaches simple Fresnel reflectances for near-grazing incidence). In the results presented here two angular ranges are used: one from 2° to 60°, the other from 2° to 42° (the 0° and 1° angles cannot be measured because the detector occludes the incident beam in the current experimental arrangement). The smaller range was studied because it corresponds to a range that could be covered by a prototype commercial scatterometer currently under development.

The experiments discussed here concentrated on the use of zeroth order data for the analyses, although the use of the ±1st orders was explored as well. As will be seen, the zeroth order signatures alone contain sufficient information about the unknown structure to yield accurate characterization of the diffracting structure. From an experimental standpoint using a single order for prediction purposes is advantageous because it minimizes the number of measurements. In addition, as the microelectronics industry pushes toward smaller device dimensions, the ±1st orders will eventually no longer exist for He–Ne illumination, making the 0th order the only choice for scatterometric measurements using 633 nm illumination.

V. DIELECTRIC GRATING LINEWIDTH MEASUREMENTS

Determination of the width, often referred to as the critical dimension (CD), is the first step in the scatterometric characterization of a submicron line in developed photoresist. If shape parameters other than linewidth are subtle to the

point of being irrelevant, this technique can provide an excellent measurement of the near-rectangular profile. Results for 1.5 μm lines in 32 μm period etched silicon structures have been published by Naqvi *et al.*[26] Large period gratings have the advantage of producing a large number of diffraction orders, whereas gratings with a 1 μm period will diffract light into only one or two orders.

Because they contain a wide variety of diffracting structures, gratings generated within a focus/exposure (F/E) matrix provide a very good test for scatterometry applications. Changes to exposure, for example, predominantly affect the linewidth while focus changes generally influence the overall shape of the resist. The linewidth measurement study was initiated with one pilot wafer with a F/E matrix printed on it; this wafer is referred to as "wafer 3." Although both the height and index of the resist was known to within a particular range, the degree of uncertainty for each was unacceptable for our model. Thus it was necessary to use the scatterometer to determine the height and index of the photoresist before predictions of any linewidths could be performed.

These two parameters can be determined from either the diffraction data or 2-Θ scans of an unpatterned region of the photoresist (i.e., a thin film). For a 2-Θ scan on a thin film, the reflected intensity goes through a minimum whenever destructive interference occurs. By generating a theoretical database of index/height combinations and comparing them via statistical algorithms to experimental scans of the photoresist, we were able to determine the index and height of the resist layer. The results matched the specified nominal values: the height was determined to be 1.00 μm, and the refractive index 1.576. In addition, from examining a patterned, diffracting sample and using zeroth order diffraction data, the MMS algorithm has been able to do a three parameter search for height, index, and linewidth. This technique determined the height to be 0.990 μm and the index 1.575.

With the two photoresist parameters determined it was possible to proceed with the analysis of grating linewidths on wafer 3. Initially we believed the sidewalls of the photoresist lines would not be perfectly square and would have some angle to them. But, when early predictions were run with the sidewall angle as a free parameter, we found the angles were being predicted at 90°, i.e., the developed lines had vertical sidewalls. Thus it was only necessary to keep one parameter free in the final prediction model: linewidth. For wafer 3 the prediction model linewidth range ran from 0.350 to 0.750 μm in 1 nm steps.

After the predictions were performed, comparisons between cross-sectional SEM and scatterometry measurements for wafer 3 showed good agreement. Unfortunately the SEM measurements were limited to six locations, three of which were useful for linewidth measurements and 3 for profile determination. These profile results are discussed in a later section. But the real impact of this one wafer pilot study was that it launched a more thorough and complete study of the scatterometry technique, with five wafers and approximation 60 top-down and 12 cross-sectional SEM measurements.

To further test the scatterometer and linewidth prediction algorithms, five sample wafers, labeled 4–8, were used. Each wafer had grating structures of 1 μm pitch and 0.5 μm

nominal linewidth. These gratings had been exposed and developed in photoresist on a silicon substrate for a range of focus and exposure values. The exposure values extended from 30 to 100 mJ in 5 mJ increments, and the focus ranged from 0 to ±1.4 μm in ±0.2 μm steps. The 2-Θ scans were performed on each of the wafers, with data collected from both the 0th and ±1st orders. The data was then used in the prediction algorithms to determine the linewidth of the grating. The calibration set was generated using the RCWT model, with the assumption that the overall grating shape was rectangular.

The effects of using different linewidth prediction algorithms for each of the wafers can be seen in Figs. 3–6. For comparison purposes, SEM measurements are included in some of the plots. Figures 3 and 4, which show the results for wafer 5, indicate very good agreement between both top-down and cross-sectional SEM and scatterometric measurements. The MMS algorithm predictions (Fig. 3) are enveloped by the top-down and cross-sectional SEM measurements over the entire exposure range. The PLS algorithm results for this wafer can be seen in Fig. 4; the results are not as close as those using MMS (particularly at low exposure energy), but they are still consistent with the SEM measurements. With regard to angular range, the 60° and 42° datasets for either statistical algorithm yield approximately the same linewidth—the most significant difference between the two occurs at the 85 mJ exposure dose.

Results for wafers 7 and 8 (Figs. 5 and 6) demonstrate less agreement with top-down SEM measurements over the entire exposure range. However, for both wafers all of the results show a clear offset between the SEM and scatterometry-measured dimensions, regardless of the prediction algorithm used. For example, the standard deviation (1σ) of the difference between SEM and scatterometry measurements (42° MMS algorithm) for wafer 7 is 7.9 nm. For wafer 8, the same algorithm results in a deviation of 8.2 nm. So, despite the offset, the scatterometry predictions are very consistent with the SEM measurements. Differences between the two techniques could perhaps be due to the effects of subtle features on the resist profiles. In other words, the theoretical model is assuming that the profiles are exactly square when, in fact, there are subtle features on the resist line that affect the scatter signatures. These complex features will be accounted for in Sec. VI.

Finally, the results for wafer 4 can be seen in Fig. 7. For this wafer two sets of top-down SEM measurements were performed. The average difference between the two SEM measurements is 12 nm. The results show approximately the same amount of offset as that for wafers 7 and 8 and are very linear with the SEM values. This can be seen in Fig. 8, which is a plot of the SEM measurements versus the scatterometry results. The correlation coefficient for the linear fit between the two techniques is 0.9922. Using the MMS 42° algorithm in comparison to SEM "b," the standard deviation (1σ) of the difference between the two measurement techniques is 7.4 nm. The average differences and standard deviations from SEM measurements for wafers 4, 5, 7, and 8 are summarized in Table I.

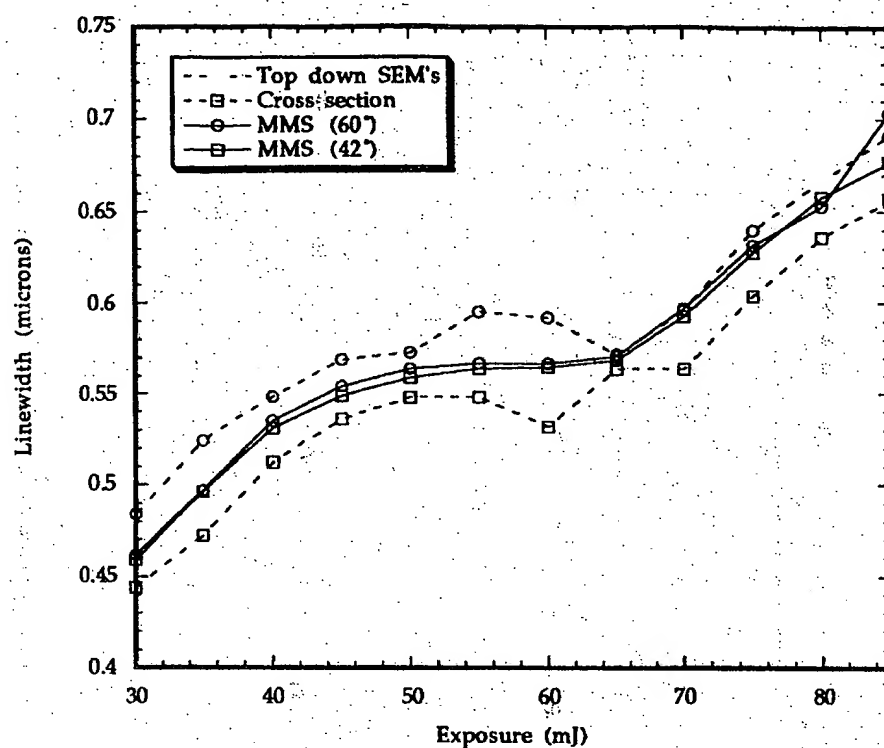The results presented thus far have all been obtained us-

FIG. 3. The MMS scatterometry results compared to top-down and cross-sectional SEM measurements for the 0 focus row on wafer 5.
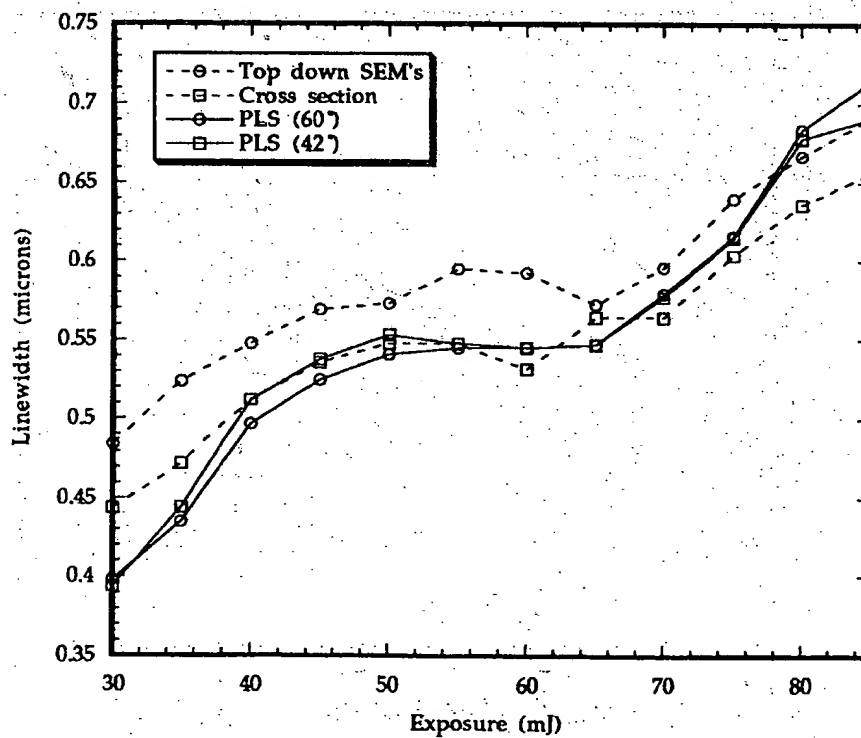

FIG. 4. The PLS scatterometry results compared to top-down and cross-sectional SEM measurements for the 0 focus row on wafer 5.
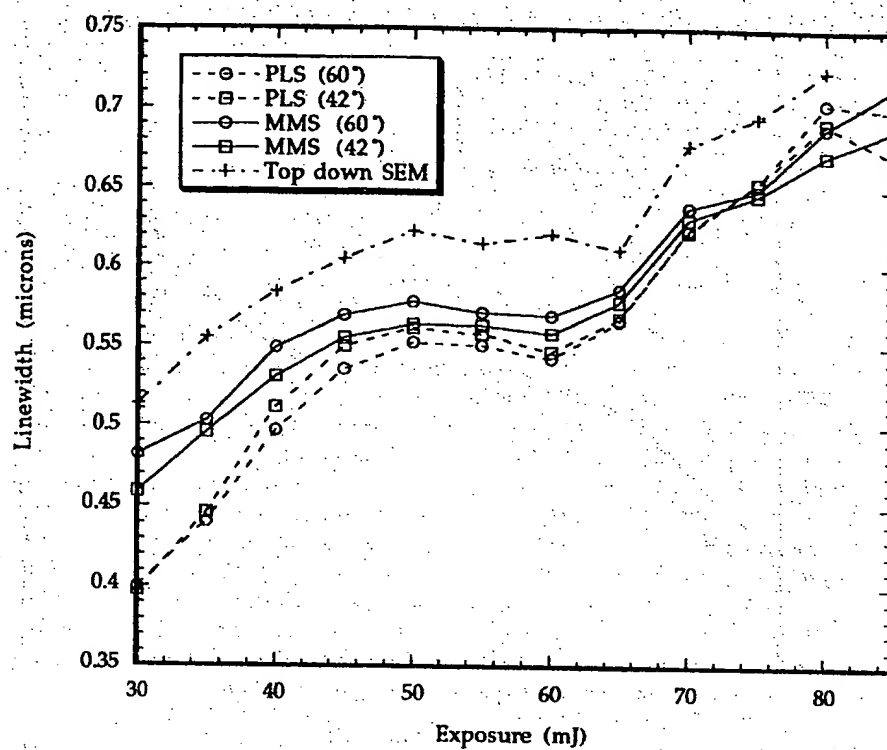
FIG. 5. The MMS and PLS scatterometry results compared to top-down SEM measurements for the 0 focus row on wafer 7.
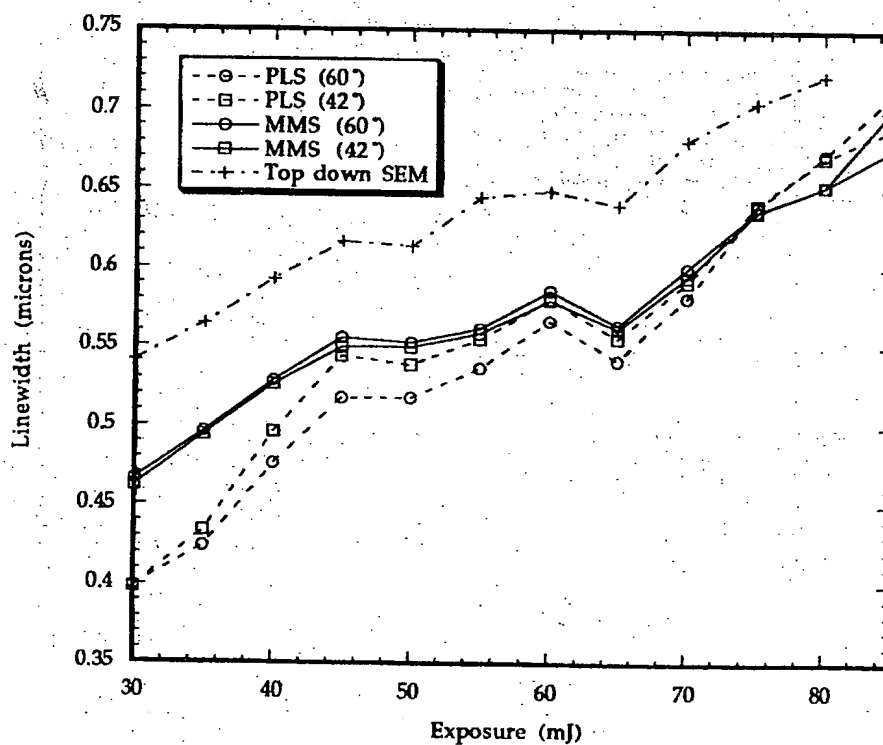

FIG. 6. The PLS and MMS scatterometry results compared to top-down SEM measurements for the +0.2 focus row on wafer 8.
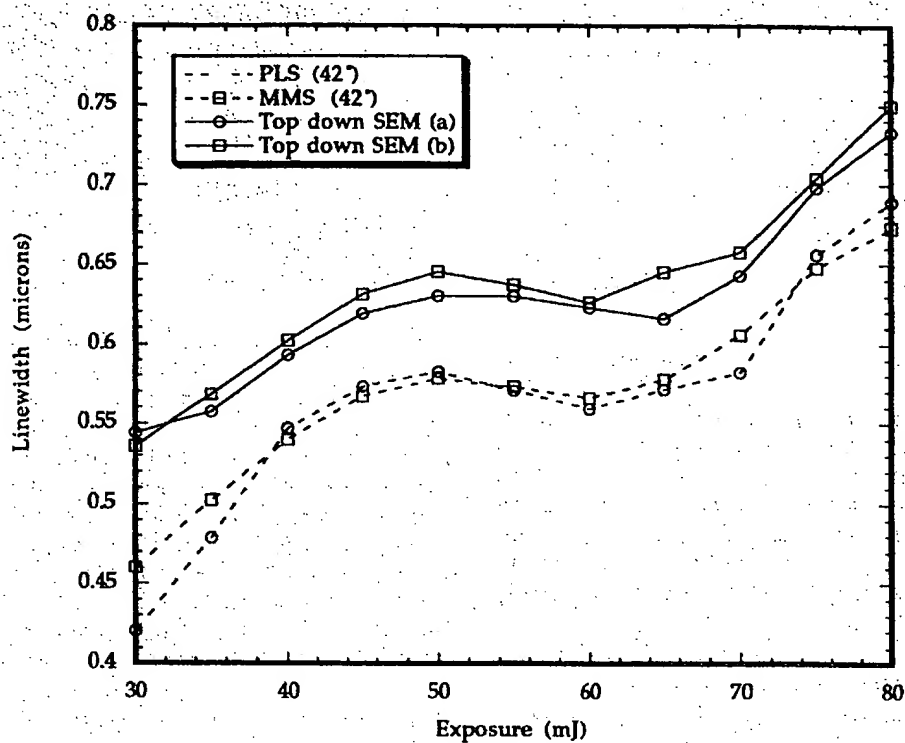
FIG. 7. The PLS and MMS scatterometry results for wafer 4, shown with two SEM measurements on the same location.
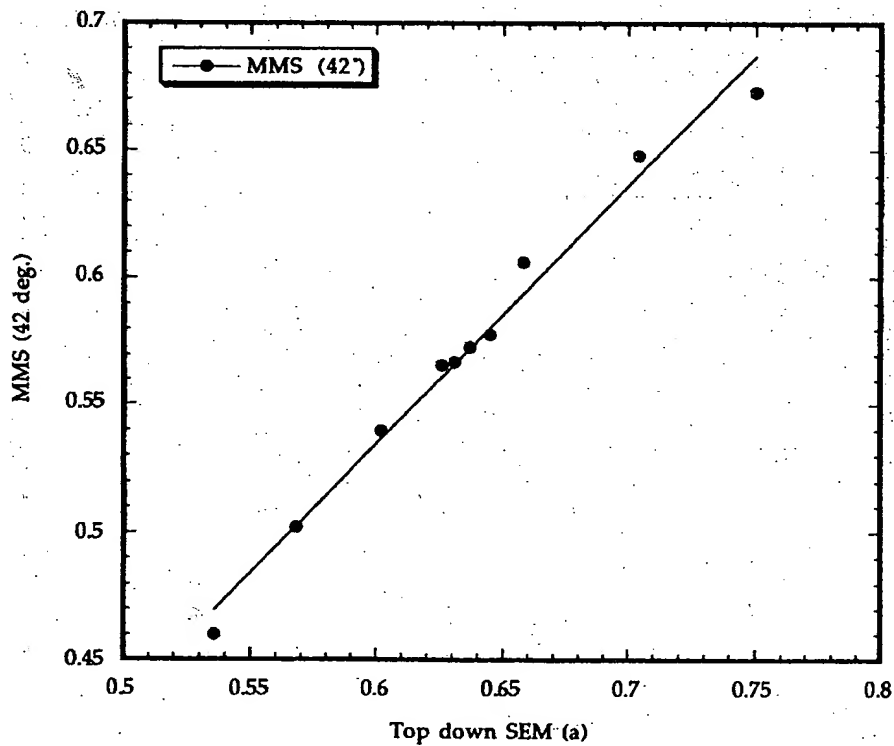

FIG. 8. The scatterometry results for wafer 4 vs the SEM measurements.

TABLE I. Summary of average differences and standard deviations. Comparison of scatterometry measurements (MMS 42°) to top-down SEM results.

Wafer I.D. No.	Average difference from SEM values	Standard deviation (1 σ) of difference from SEM values
4	54.0 nm (trial a)	12.3 nm (trial a)
4	64.6 (trial b)	7.4 (trial b)
5	16.9	9.4
7	52.0	7.9
8	73.3	8.2

FIG. 10. The slicing technique used to accommodate an arbitrary grating profile.

ing the zeroth diffraction order. However, for gratings having a 1 μm period, the first diffracted order can also be used for characterization (or monitoring). Figure 9 shows the results of using first order data to predict linewidths of wafer 5. Although the PLS results differ from the SEM results at higher linewidths, the MMS results are consistent with the SEM results for the entire range. The excellent agreement between the first order data and experimental results bolsters our confidence in the use of the theoretical model to predict grating shape parameters.

VI. COMPLEX STRUCTURE ANALYSIS

In addition to the primary parameters of interest associated with gratings, such as period and linewidth, it is possible that more complex structural shapes, such as rounded corners and nonrectangular profiles, may be detected and characterized by 2-Θ scatterometry. Such irregular shapes

are common in the production of submicron structures of photoresist since even slight changes in focus and/or exposure conditions can have a significant effect on the photoresist profile once it is developed.

We adapted our model to accommodate an arbitrary grating profile and generated a library of scatter signatures from complex profiles. The data were generated by slicing each profile into many layers of thin rectangular slabs, and then running the theoretical model over all the layers while applying the appropriate boundary conditions at each interface. In this manner a rounded grating profile is approximated by a number of thin rectangular gratings stacked one upon the other. This technique has been used in the past to predict the dimensions of trapezoidal resist profiles with success.[28]

Two common features encountered in submicron photoresist structures are rounded top and bottom corners. Figure 10 illustrates how this particular type of profile is sliced into different layers. Note that any regions with vertical sidewalls
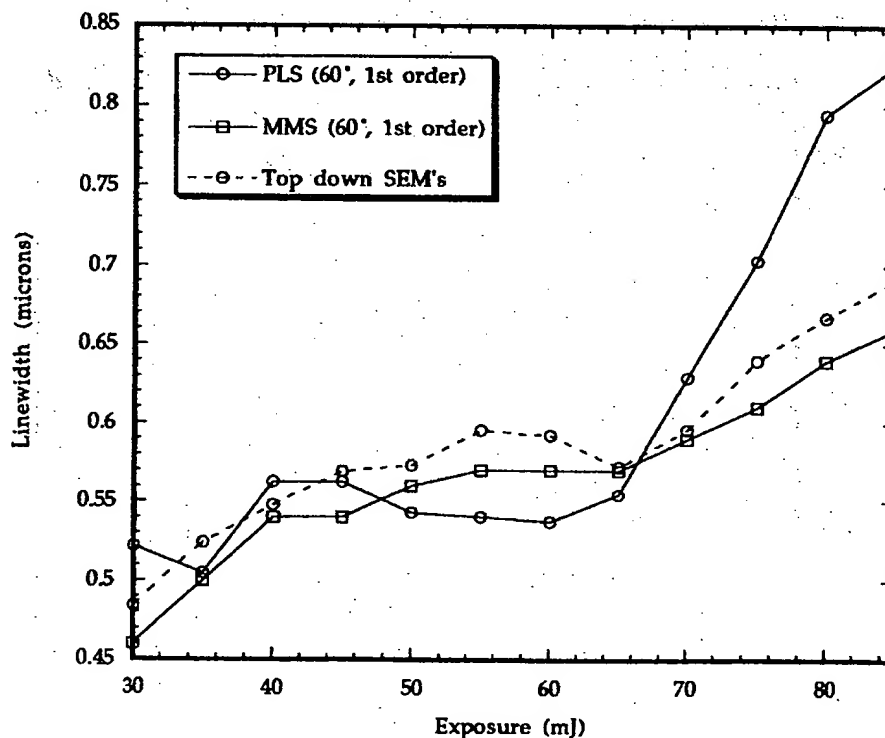

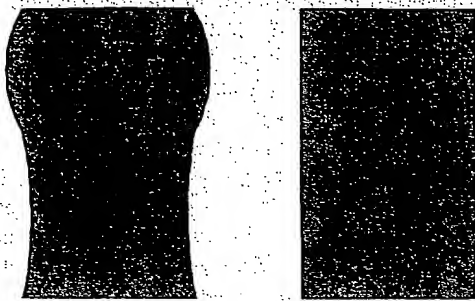FIG. 9. Prediction results using first order data.

FIG. 11. Irregular vs square profiles used in the prediction algorithms, shown here proportionally to scale.

FIG. 12. Theoretical scatter signatures for square and irregular shaped profiles compared with the experimental signature.

need only to be represented by one layer. The shape of the round portion of each corner is simply a quarter circle of a given radius. A range of corner radii was used in conjunction with the previously predicted nominal linewidth to establish the theoretical library. Then the MMS statistical algorithm was implemented to determine the best match between theory and experiment, and thus predict the radius of either corner. Due to the nature of the chemically amplified resist being used, the dimensions of the radii were very small. Nevertheless, analyzing profiles with such small dimensions (~10 nm) provided a rigorous test for the theoretical model and prediction algorithm.

The prediction process for the profiles was done in two steps. First, the vertical structure library was used to find the linewidth of each profile, as previously illustrated. Then, using this predicted linewidth, the MMS algorithm was run for both the top and bottom corner radii of the profiles. By proceeding in this manner, we were able to limit our final parameter space to just the two corner radii. This drastically reduced the computing time required to generate the theoretical parameter space. For example, to search over three parameters with ten incremental values per parameter would require 1000 theoretical data files. But to limit the search to two parameters results in only 100 files.

Cross-sectional SEMs were performed on four of the die locations. Three of the locations were used to determine actual dimensions related to the overall profile. The fourth location, for which the stepper was defocused intentionally, possessed a very complicated profile and was not parameterized in the usual manner. Instead, the dimensions of the profile were taken from the original SEM picture [Fig. 13(a)] and implemented into the theoretical model. A scatter signature corresponding to this profile was then generated, and
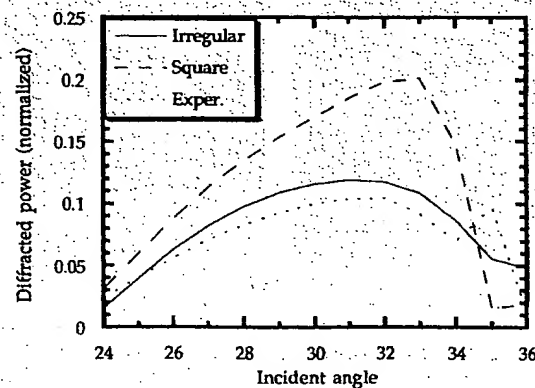
comparisons were made with the actual experimental data. This technique for modeling complex photoresist gratings has also been used successfully by Moharam et al.[35]

For this irregular shape, shown as it was modeled theoretically (Fig. 11) in proportion to a square profile, the mean square error using 0th order data from 0° to 60° incidence angle was 12% lower than for the square profile. Thus a statistical algorithm would predict the irregular shape as being the more representative one. So, despite the fact that the shape has overhanging sidewalls, the structure is very well characterized by scatterometry. This feature would go undetected by other techniques apart from cross-sectional SEM and the very latest profilometry techniques. Figure 12 shows a plot of the theoretical scatter signatures and the experimental data taken from the location known to have the irregular profile. The particular angular range plotted accounts for most of the 12% error difference. Clearly the irregular profile shows better agreement with the data, illustrating the ability of scatterometry to detect this type of shape.

Regarding the remaining three locations, the dimensions of the radii on the top and bottom corners were determined, and comparisons were made to SEMs. While the dimensions determined by scatterometry are exact in a computational sense, the cross-sectional SEM photos used for comparison purposes were difficult to interpret. Because the curvatures of the corners were so small, these features could only be *estimated* from the SEM pictures using a reticled inspection lupe. Although these estimates are subjective and prone to error, the comparison shows reasonably good agreement between scatterometry and cross-sectional SEM measurements.

TABLE II. Results of complex profile measurements.

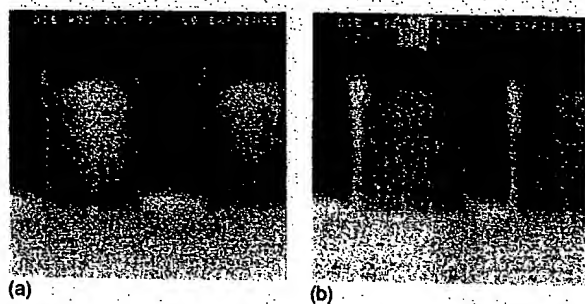| Exposure/ Location	Top corner radii		Bottom corner radii	
	Scatterometry	SEM estimate	Scatterometry	SEM estimate
30 mJ, location A	0.00 μm	No apparent radius	0.00 μm	No apparent radius
60 mJ, location G	0.09 μm	~0.04±0.03 μm	0.00 μm	No apparent radius
90 mJ, location M	0.10 μm	~0.08±0.03 μm	0.07 μm	~0.03±0.03 μm

FIG. 13. (a) The "inverted S"-shaped profile. (b) The 90 mJ location, with both top and bottom rounded corners.

The results can be seen in Table II. Figure 13(b) shows the SEM picture for the 90 mJ location.

VII. LIMITS OF APPLICATION

In today's production lines, 0.5 μm fabrication technology is already standard for high-end commercial semiconductor devices. In order to keep pace with the industry, it is essential that the techniques discussed here will be applicable to dimensions well below 0.5 μm.

The performance of these prediction methods on smaller dimensions was evaluated by generating theoretical scatter signatures for 0.24 μm pitch/0.12 μm linewidth photoresist on Si structures. The illuminating wavelength was 442 nm, corresponding to the output of a He–Cd laser. Using the resulting angular diffraction signatures, a prediction method similar to the PLS algorithm was simulated. The results showed that the standard deviation (1σ) in the prediction was 5 nm. In addition, we are currently investigating actual 0.24 and 0.35 μm structures using 633 nm illumination wavelength. Early results are encouraging, and it seems reasonable to assume that scatterometry, while using convenient, visible wavelengths, will prove viable even as feature sizes decrease below 0.1 μm several years in the future.

VIII. REPEATABILITY

The repeatability of an instrument can be defined as the variation of measured values when a sample is measured repeatedly under constant conditions with that instrument.[1] Repeatability is commonly expressed in multiples of the standard deviation, σ, of the repeated measurements. For measuring 0.5 μm features created with a linewidth control of 10%, the required 3σ measurement repeatability is one-third of the linewidth control, or 16 nm. Accuracy is often defined as the agreement of a measured value of the "true values"[1,36] or to an accepted reference value such as a NIST standard. Accurate measurements require a set of standards for the instrument in question; unfortunately, submicron standards are not available in many cases. However, the ability to measure accurately is not always as critical as the ability to measure repeatably. For example, an instrument with good repeatability and linearity can detect changes in the process environment. Often, this is all that is required for processing applications.

To determine the repeatability of the 2-Θ scatterometer, three experiments were performed. The first was designed to test the short-term repeatability of the instrument. In this experiment 30 consecutive zeroth order 2-Θ scans were performed on the same day on the same part of the sample (the wafer was never removed from its mount). For each scan we obtained a prediction of the linewidth (using the PLS and MMS routines, 60° and 42° data sets) and calculated the mean and standard deviation for the set of measurements.

The second experiment, which was designed to determine the day-to-day repeatability of the scatterometer, involved seven measurements over seven days on the same wafer location. In this experiment the entire scatterometer was started cold each day; the sample was removed and repositioned on a daily basis. Factors that would affect this type of repeatability are mostly due to operator subjectivity when the sample is positioned because of variations across the grating.

Finally, the third experiment was conducted after the entire scatterometer optical system was removed, upgraded and realigned. This presumably represents the worst possible situation in terms of repeatability. The scans were made on the same location as in the first two experiments.

For each experiment the linewidth of the grating was determined using the standard four prediction algorithms. The average and standard deviation associated with each experiment was then calculated. The results, seen in Table III, show that the scatterometer demonstrates very good repeatability, i.e., a very low standard deviation. For the short-term study, the worst 1 σ is 2.0 nm; at best, it is 0.5 nm (using the 42° MMS algorithm). For the day-to-day repeatability the worst case is slightly higher at 4.0 nm, as expected. The best day-to-day repeatability is 0.8 nm, which once again corresponds to the 42° MMS algorithm.

For purposes here the standard deviation σ is defined to be

$$\sigma = \sqrt{\frac{\sum_{i=1}^{N} (x_i - \bar{x})^2}{N-1}}. \tag{2}$$

Recently a new technique for grating linewidth measurements using an environmental scanning electron microscope (ESEM) was reported.[37] The ESEM was used in order to eliminate the charging effects associated with insulating materials such as photoresist when they are used in a conventional SEM. These charging effects can have an adverse affect on the linewidth measurement. The ESEM study used a sample that was comparable to ours: a 1.0-μm-thick photoresist layer on Si with a nominally 0.5 μm linewidth. The ESEM's static 1σ repeatability, taken from 10 measurements, was 1.3 nm. The day-to-day repeatability was not cited, but was presented in a graphical form. From interpolation of two of these data plots we have determined the 1 σ day-to-day repeatability to be 1.6 and 2.7 nm, respectively. Thus the scatterometric techniques presented here have repeatability figures that are as good as, or better than, the latest SEM techniques.

TABLE III. Results of the repeatability study. (Dimensions are in nanometers.)

Algorithm	Repeatability type	Average linewidth	1σ
PLS 60	Short term, same day	541.4	2.0
	Day to day	548.3	4.0
	Complete rebuild	567.9	n/a
PLS 42	Short term, same day	551.1	2.8
	Day to day	563.9	3.2
	Complete rebuild	567.9	n/a
MMS 60	Short term, same day	559.2	0.8
	Day to day	569.7	1.0
	Complete rebuild	571.0	n/a
MMS 42	Short term, same day	564.7	0.5
	Day to day	565.0	0.8
	Complete rebuild	567.0	n/a

IX. CONCLUSIONS

We have demonstrated that 2-Θ scatterometry is capable of accurately determining the linewidth of developed photoresist gratings. In addition, the same techniques can be applied to determine the more subtle features of the resist lines such as rounded corners or overall shape. Comparisons between scatterometric and SEM measurements show good agreement for both linewidth and profile measurements. Furthermore, the precision of the scatterometer has been demonstrated to be excellent, as is evidenced by its low standard deviation. In fact, the repeatability of the scatterometer is comparable to the best metrology tools available and is significantly lower than a recent, novel SEM technique.

Characterizing the line shape of developed resist gratings is just the first step in using scatterometry as a new metrology method. Indeed, in order for scatterometry to be used in a semiconductor manufacturing environment there are other process variables that must be taken into account. For example, if there are underlying films that have thickness variations from wafer to wafer, linewidth predictions will be affected if these variations are not included in the theoretical calibration model.

At present we are investigating a large, 25 wafer sample set to determine how additional process parameters affect scatterometer measurements. In this experiment, intentional variations have been introduced into several of the process steps, resulting in a sample set which mimics real process drift. Scatterometer measurements are being made for all the varying parameters. We will report these results in a future publication.

ACKNOWLEDGMENTS

[1] T. R. Corle, Solid-State Electron. 35, 391 (1992).
[2] W. L. Stevenson, Proc. SPIE 921, 352 (1988).
[3] M. Davidson, Microelectron. Eng. 13, 523 (1991).
[4] R. Iscoff, Semicond. Int. 17, 56 (1994).
[5] R. Toledo-Crow, B. W. Smith, J. K. Rogers, and M. Vaez-Iravani, in
Integrated Circuit Metrology, Inspection, and Process Control VIII (SPIE, Bellingham, WA, 1994).
[6] J. E. Griffith and D. A. Grigg, J. Appl. Phys. 74, R83 (1993).
[7] G. Binnig, C. Gerber, E. Stoll, T. R. Albrecht, and C. F. Quate, Europhys. Lett. 3, 1281 (1987).
[8] S. Manne, H. J. Butt, S. A. C. Gould, and P. K. Hansma, Appl. Phys. Lett. 56, 1758 (1990).
[9] G. Meyer and N. M. Amer, Appl. Phys. Lett. 58, 2100 (1990).
[10] P. Dietz, C. A. Ramos, and P. K. Hansma, J. Vac. Sci. Technol. B 10, 741 (1992).
[11] D. Nyyssonen, in *Integrated Circuit Metrology, Inspection, and Process Control VII* (SPIE, Bellingham, WA, 1993), pp. 325–335.
[12] M. T. Postek and D. C. Joy, Solid State Technol. 29, 145 (1986).
[13] R. R. Hershey and M. B. Weller, Proc. SPIE 1926, 287 (1993).
[14] J. R. Lowney, M. T. Postek, and A. E. Vladar, in Ref. 5, pp. 85–96.
[15] K. M. Monahan, G. Toro-Lira, and M. P. Davidson, in Ref. 11, pp. 336–346.
[16] M. T. Postek, A. E. Vladar, S. N. Jones, and W. J. Keery, Proc. SPIE 1926, 268 (1993).
[17] L. A. Firstein and A. Noz, in *Integrated Circuit Metrology, Inspection, and Process Control V* (SPIE, Bellingham, WA, 1991), pp. 81–88.
[18] S. S. H. Naqvi, S. H. Zaidi, S. R. J. Brueck, and J. R. McNeil, J. Vac. Sci. Technol. B 12, 3600 (1994).
[19] J. R. McNeil et al., Microlithog. World 1, 16 (1992).
[20] S. Wittekoek et al., Proc. SPIE 22 (1985).
[21] R. Pforr et al., in *Optical/Laser Microlithography V* (SPIE, Bellingham, WA, 1992), pp. 594–608.
[22] M. P. Lang, M.S., University of New Mexico, 1992.
[23] L. M. Milner, K. P. Bishop, S. S. H. Naqvi, and J. R. McNeil, J. Vac. Sci. Technol. B 11, 1258 (1993).
[24] K. C. Hickman et al., J. Vac. Sci. Technol. B 10, 2259 (1992).
[25] J. Sturtevant, S. Holmes, and P. Rabidoux, in *Advances in Resist Technology and Processing IX* (SPIE, Bellingham, WA, 1992), pp. 114–124.
[26] S. S. H. Naqvi et al., J. Opt. Soc. Am. A 11, 2485 (1994).
[27] S. S. H. Naqvi, J. R. McNeil, R. H. Krukar, and K. P. Bishop, Microlithog. World 2, 5 (1993).
[28] K. P. Bishop, S. M. Gaspar, L. M. Milner, S. S. H. Naqvi, and J. R. McNeil, *Proceedings of the International Conference on the Application and Theory of Periodic Structures* (SPIE, Bellingham, WA, 1991), pp. 64–73.
[29] S. S. H. Naqvi, S. M. Gaspar, K. C. Hickman, and J. R. McNeil, Appl. Opt. 31, 1377 (1992).
[30] R. Petit, in *Topics in Current Physics* (Springer, Berlin, 1980).
[31] T. K. Gaylord and M. G. Moharram, Proc. IEEE 73, 894 (1985).
[32] R. H. Krukar et al., Proc. SPIE 1926, 60 (1993).
[33] E. V. Thomas and D. M. Haaland, Anal. Chem. 62, 1091 (1990).
[34] D. M. Haaland and E. V. Thomas, Anal. Chem. 60, 1193 (1988).
[35] M. G. Moharram, T. K. Gaylord, G. T. Sincerbox, H. Werlich, and B. Yung, Appl. Opt. 23, 3214 (1984).
[36] *1986 Annual Book of ASTM Standards* (American Society for Testing and Materials, Philadelphia, 1986, Designation E).
[37] T. Yamaguchi, S. Kawata, S. Suzuki, T. Sato, and Y. Sato, Jpn. J. Appl. Phys. Part 1 32, 6277 (1993).